Original Article
miR-19a mediates the mechanism by which SPHK2 regulates hypopharyngeal squamous cell carcinoma progression through the PI3K/AKT axis

Ji Song[1,2], Yanshi Li[2], Tao Lu[2], Min Pan[2], Zhihai Wang[2], Chuan Liu[2], Yang Liao[1], Guohua Hu[2]

[1]Department of Otorhinolaryngology, The University-Town Hospital of Chongqing Medical University, Chongqing, China; [2]Department of Otorhinolaryngology, The First Affiliated Hospital of Chongqing Medical University, No. 1 Youyi Road, Yuzhong District, Chongqing, China

Abstract: This study explored the expression of sphingosine kinase 2 (SPHK2) and microRNA miR-19a-3p (miR-19a-3p) in patients with Hypopharyngeal squamous cell carcinoma (HSCC) together with pathways affecting HSCC invasion and metastasis. Quantitative real-time polymerase chain reaction (qRT-PCR) and Western blotting (WB) were performed to assess the differential expression of SPHK2 and miR-19a-3p in patients with HSCC lymph node metastasis (LNM). Immunohistochemical (IHC) results were analyzed together with clinical information to evaluate their clinical significance. Subsequently, the functional effects of SPHK2 overexpression and knockdown on FaDu cells were evaluated in in vitro experiments. We performed in vivo experiments using nude mouse to assess the effects of SPHK2 knockdown on tumor formation, growth and LNM. Finally, we explored upstream and downstream signaling pathways associated with SPHK2 in HSCC. SPHK2 was significantly elevated in HSCC patients with LNM and survival was lower in patients with enhanced SPHK2 expression (P < 0.05). We also demonstrated that SPHK2 overexpression accelerated the proliferation, migration, and invasion. Using animal models, we further verified that SPHK2 deletion abrogated tumor growth and LNM. In terms of mechanism, we found that miR-19a-3p was significantly reduced in HSCC patients with LNM and was negatively associated with SPHK2. MiR-19a-3p and SPHK2 could regulate tumor proliferation and invasion through the PI3K/AKT axis. SPHK2 was found to contribute significantly to both LNM and HSCC patient prognosis and was shown to be an independent risk factor for LNM and staging in HSCC patients. The miR-19a-3p/SPHK2/PI3K/AKT axis was found to contribute to the development and outcome of HSCC.

Keywords: SPHK2, hypopharyngeal squamous cell carcinoma, lymph node metastasis, miRNA-19a-3p, PI3P/AKT pathway

Introduction

Head and neck malignancies rank sixth in the incidence of systemic malignancies. Ninety percent of head and neck malignancies are squamous cell carcinomas, of which hypopharyngeal squamous cell carcinoma (HSCC) has one of the worst prognoses of these cancers [1]. Without treatment, fewer than 20% of patients survive for 12 months, with survival closely related to the anatomical location of the hypopharynx. Early identification and radical therapy are crucial to the management of malignant tumors. However, due to the tumor's insidious early clinical features, most HSCC patients already have advanced disease at diagnosis. As a result, approximately 60-80% of HSCC patients exhibit lymph node metastases (LNM) when starting treatment [2]. However, while improved diagnosis and treatment can increase the effectiveness of primary tumor management in HSCC, the 5-year overall survival (OS) rate is only 13-50%, without marked improvement over the last decade [3, 4]. A series of investigations revealed that HSCC with LNM is a stand-alone risk factor (RF) for patient mortality and a major contributor to treatment failure [5, 6]. Therefore, the identification of new effective therapeutic targets, the exploration of indicators and biomarkers for the assessment of

prognosis and treatment sensitivity, and improving patients' long-term survival are key to the treatment of HSCC at present.

In recent years, researchers have identified numerous molecules related to the invasion and migration of HSCC, as well as subsequent metastasis, using gene sequencing techniques. Such molecules include VEGF, CCR7, Syk, and EGFR [7, 8]. In prior investigations, our group employed gene sequencing technology to sequence the entire transcriptome of three pairs of HSCC patients (three with and three without metastasis) to identify differentially expressed genes (DEGs) affecting LNM. A significant association between sphingosine kinase 2 (SPHK2) and LNM was found. Various studies have demonstrated the involvement of SPHK2, a key target in the sphingolipid metabolic pathway, in tumor development, with aberrant expression linked with both tumorigenesis and metastasis [9-13]. For example, SPHK2 overexpression has been found to be strongly correlated with poor prognosis, LNM, or distant metastasis in lung, breast, gastric, and colorectal cancers [14-20]. However, there is no information on the involvement of SPHK2 with HSCC. The present study investigated this association through the retrospective analysis of patient information as well as laboratory results.

The phosphatidylinositol 3-kinase (PI3K) axis is often associated with human cancers, and its activation has been linked to both tumorigenesis and tumor progression [21]. Many studies have investigated the protein kinase AKT and its significance in mediating PI3K signaling. This signal transduction network regulates multiple cellular processes, namely, proliferation, adhesion, migration, invasion, metabolism, and survival [22], and it is highly expressed in a variety of tumors, including ovarian, prostate, esophageal, and gastric cancers [23-26]. However, these pathways have not been investigated in HSCC. To further explore the mechanism by which SPHK2 promotes HSCC development, we conducted a series of mechanistic studies and investigated the potential downstream mechanisms. Based on the results of bioinformatics analyses, it was predicted that SPHK2 can influence the development and metastasis of HSCC through the PI3K/AKT pathway. This was further verified for the first time in cellular experiments.

MicroRNAs (miRNAs) are a class of endogenous non-coding single-stranded RNAs that regulate mRNA translation. Overexpression of several miRNAs has been shown to promote tumor metastasis via multiple signaling pathways associated with the epithelial-mesenchymal transition (EMT) and autophagy, amongst others, in tumor cells [27]. Here, we used miRNAs to examine upstream signaling pathways associated with LNM in HSCC patients. We searched three scientific databases, namely, TarBase, miRDB, and TargetScan to identify SPHK2-targeting miRNAs and, from the miRNAs identified by all three databases, selected miR-19a-3p and miR-19b-3p for further investigation. Aberrant expression of miR-19a-3p has been reported in various tumors [28] and it is closely associated with the PI3K/AKT signaling network [29], reported to mediate PI3K/AKT signaling in gastric, colorectal, breast, thyroid, and bladder cancers [30-34]. Nevertheless, the specific details of its role in HSCC, including LNM, are not fully understood. After confirming the expression of miR-19a-3p in patients with HSCC, we further verified the findings in in vitro experiments to further clarify the details of the mechanism.

Thus, the objectives of this study were to elucidate the expression of SPHK2 and microRNA miR-19a-3p in patients with hypopharyngeal carcinoma, as well as to determine their differential expression in patients with and without lymph node metastasis.

Materials and methods

Clinical data

Samples of tumor and adjacent normal mucosal tissue were collected from HSCC patients who underwent surgery at the Department of Otolaryngology, The First Affiliated Hospital of Chongqing Medical University between 2012 and 2020. The inclusion criteria were patients (1) With a confirmed pathological HSCC diagnosis, (2) Receiving first treatment, as per NCCN guidelines, (3) AJCC TNM classification (8th edition)-based clinical staging, and (4) Who had undergone electron laryngoscopy, as well as CT or MRI, every six months following the initial surgery, with complete follow-up records to the cut-off date of the study or death. The following patients were excluded from the analysis: (1) HSCC patients who had undergone

radio- or chemotherapy prior to surgery; (2) Patients with other tumors. All participants provided written informed consent to the procedure and related experimental content before treatment. The study was approved by Chongqing Medical University and followed the strict guidelines of the World Medical Association Ethics Code. Ultimately, 57 HSCC patients who fulfilled the above criteria were selected for analysis.

Experimental reagents and materials

Primers were designed and synthesized by Invitrogen (Beijing, China). The FaDu HSCC cell line was acquired from the Shanghai Cell Bank, Chinese Academy of Sciences. The lentiviral silencing and overexpression plasmids were obtained from Gikai Shanghai. The SPHK2 antibody, the p-AKT 308 antibody, the p-AKT 473 antibody, the AKT antibody, antigen repair solution, and rabbit anti-human SPHK2 monoclonal antibody were purchased from Abcam (Cambridge, UK), the PI3K p110α antibody were purchased from Polyclonal antibody (Proteintech, US), and the goat anti-rabbit IgG secondary antibody from Wuhan Boost Biotechnology Co., Ltd. (Wuhan, China). The SP kit (SP-9000), DAB kit (concentrated) (ZhongShan JinQiao Company, Beijing, China), ethanol (100%), xylene, methanol, Juan-based salicylic acid, trichloroacetic acid, and sodium chloride were obtained from Sinopharm Chemical Reagent Co., Ltd. (China), Dulbecco's Modified Eagle Medium (DMEM) high-sugar medium, and fetal bovine serum were from Gibco (Waltham, MA, USA), phosphate-buffered saline (PBS), trypsin, and crystal violet staining solution were from Mengbio (China), and the penicillin-streptomycin mixture, fluorescein K+ salt, puromycin, DAPI staining solution, and the fluorescent quencher were obtained from Biyuntian (China). PI3K/AKT inhibitor (LY294-002) were from, Med Chem Express, USA.

Cell culture, passaging, and transfection

Resuscitated FaDu cells were grown in DMEM complete medium in an incubator at 37°C and 5% CO_2 incubator and passaged when confluent. For transfection, cells in the logarithmic growth phase were collected and incubated with the lentiviral vector and virus infection reagent at 37°C and 5% CO_2, following the kit directions. After 48-72 h, stably transfected FaDu cells were selected, cultured, passaged, then frozen.

Assessment methods

Immunohistochemistry: Pre-prepared paraffin-embedded tissues were sliced into 4-μm sections. The sections were dewaxed in fresh xylene and rehydrated in an ethanol gradient, followed by antigen repair with citrate buffer at 100°C for 30 min, and overnight (ON) incubation in a 1:200 dilution of anti-SPHK2 antibody. The sections were then rinsed three times in PBS on a shaker, followed by incubation with diaminobenzidine (DAB) (ZSGB-BIO, China) for 5 min for visualization of the antigen-antibody reaction. The sections were then stained with hematoxylin for 60 seconds and washed for 10 min in distilled water before dehydration in xylene and alcohol gradients and covering them with coverslips. Normal mucosal tissue was used as the positive control and the replacement of the primary antibody by PBS as the negative control. The stained sections were independently scored by two pathologists as follows: negative SPHK2 expression (no or scarce staining, ≤ 50% of tumor cells) or positive SPHK2 expression (moderate or strong staining, > 50% of tumor cells), depending on the area and intensity of staining.

Quantitative PCR (qPCR): Total RNA was extracted from the cells and tissues using TRIzol. Ten nanograms of RNA were used in subsequent reactions using the TaqMan miRNA Assay (Applied Biosystems, Waltham, MA, USA) with incubations at 16°C for 30 min, 42°C for 30 min, and 85°C for 5 min, before storage at 4°C. Real-time PCR (RT-PCR) reactions were conducted at 95°C, 5 s at 95°C, and 40 s at 60°C for 40 cycles. U6 was used as an endogenous control for miR-19a-3p, and 18S rRNA for SPHK2. The primer sequences are shown in **Table 1**. The RT-PCR reactions were carried out in triplicate. The qPCR amplification and dissociation curves were assessed, and the relative expression of the target genes was calculated using the $2^{-\Delta\Delta CT}$ formula.

Western blotting (WB): Total protein was isolated from cells and tissues using radioimmunoprecipitation assay (RIPA) buffer from the Total Protein Extraction Kit (KeyGen Biotechnology, China). Equal amounts of proteins were separated on 10% SDS-PAGE and transferred to PVDF membranes. The membranes were blocked for 1 h in 5% skimmed milk at room temperature (RT), followed by ON incubation

Table 1. Primer sequences

Name	Primer Sequence (5'-3')
SPHK2	F: CCCGGTTGCTTCTATTG
	R: ACAGCTTCCTCCCAGTCA
18srRNA	F: GGAGTCAACGGATTTGGT
	R: GTGATGGGATTTCCATTGAT
miR-19a	F: GCAGTCCTCTGTTAGTTTTGC
	R: GCAGGCCACCATCAGTTTT
U6	F: CTCGCTTCGGCAGCACATATACT
	R: ACGCTTCACGAATTTGCGTGTC

Abbreviations: F, forward; R, reverse.

with the primary antibodies on a shaker at 4°C. Following three rinses in PBST, the membranes were incubated with secondary goat anti-rabbit IgG antibodies (Beyotime, 1:5000, China), rinsed three times in PBST for 10 min each, and visualized using the ECL system (Pierce, Thermo, USA).

CCK-8 assays: Cell viability was determined using the CCK-8 assay. Cells (approximately 10,000 cells per well) were seeded in 96-well plates with five biological replicates per treatment, and incubated at 37°C and 5% CO_2 for 24-72 h to facilitate adhesion. The medium was replaced with fresh medium, and the plates were maintained at 37°C for an additional 24 h, after which 20 ul of the CCK-8 reagent was added to each well and incubated for 0.5-2 h before measurement of the absorbance at 450 nm using an enzyme marker. Cell viability was also measured at 48 and 72 h.

Colony formation assay: To evaluate cell proliferation, we seeded 1000 cells transfected with specified plasmids for 48 h, into the wells of 6-well plates. The cells were allowed to grow in medium supplemented with 10% FBS for approximately 2 weeks with a medium change every 3 days. The cells were then fixed with anhydrous formaldehyde, followed by staining with 0.5% crystal violet. Colonies were counted under an inverted microscope. Colonies containing more than 10 cells were counted, and the colony formation rate was calculated as the (number of clones/number of inoculated cells) *100%.

Transwell migration and invasion assay: Cells were transfected for 24 h, after which they were harvested and seeded into 24-well plates at 3 × 10⁴ cells/well. The cells were then

removed with pancreatin, and 200 μL of the cell suspension was introduced to the top chamber of the Transwell plate while 600 μL of DMEM with 10% FBS was added to the lower chamber. After incubation at 37°C for 48 h, the unmigrated cells were removed from the top chamber, and the plate was rinsed three times in PBS, the cells were fixed in 4% paraformaldehyde for 10 min, followed by three rinses in double-distilled water. The cells were then stained with 0.5% crystal violet and the number of invasive cells was evaluated under a microscope.

Animal experiments: To establish the BALB/cA-nu nude mouse HSCC footpad tumorigenesis model, 4-week-old male immunodeficient BALB/cA-nu mice between 18-20 g in weight were used. The BALB/cA-nu nude mice were purchased from Spelford (China). Two groups of five mice each were established, namely, the blank plasmid cell injection group (sh-SPHK2-NC) and an experimental group (sh-SPHK2), and the corresponding cell suspensions were injected into the foot pads of the mice. The mice were euthanized after 35 days and the primary foot pad tumor and popliteal lymphatic metastases were extracted to measure the tumor weights and volumes, and the popliteal lymph node count and weight for statistical analysis, respectively.

Statistical analysis: Graph Pad Prism 8 software was used to analyze the data. All experiments were repeated at least three times. The data were evaluated by one-way ANOVA or Student's t-test and presented as the mean ± SD. $P < 0.05$ indicated that the results were statistically significant.

Results

SPHK2 levels are associated with LNM of HSCC

Our previous whole-transcriptome sequencing revealed that SPHK2 was a significant DEG in HSCC tissues. To verify its enhanced expression in HSCC samples, we measured its expression with q-PCR and WB. These showed that both mRNA and protein expression of SPHK2 was markedly increased in HSCC samples, relative to healthy controls ($P < 0.001$). Moreover, the SPHK2 content was elevated in
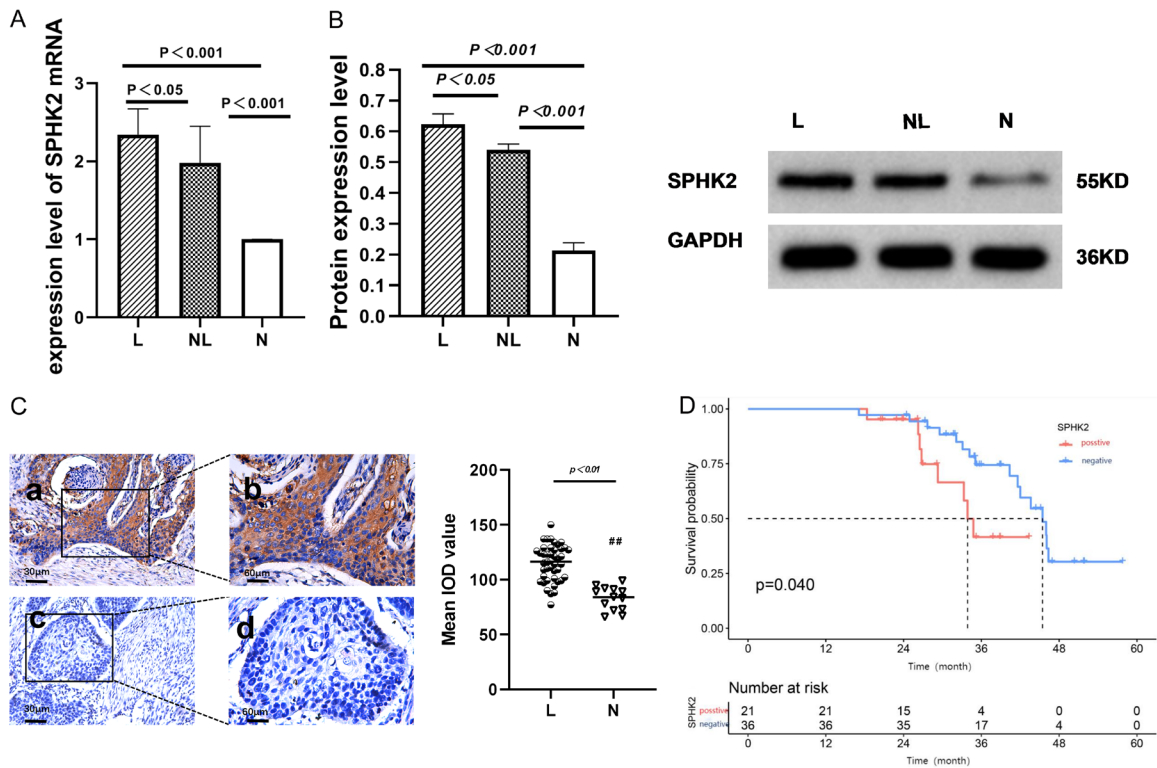
Figure 1. The expression of SPHK2 in HSCC patients and its associated prognosis. A. mRNA expression levels of SPHK2 were detected by qRT-PCR in HSCC tissues (10 samples from HSCC patients with LN metastasis patients and another 10 from patients without LN metastasis) and 10 corresponding adjacent normal tissues; B. SPHK2 protein expression was detected by WB in HSCC tissues (6 samples from HSCC patients with LN metastasis patients and another 6 from patients without LN metastasis) and 6 corresponding adjacent normal tissues; C. The immuno-histochemical results of SPHK2 staining were as follows: a. Positive immunohistochemistry in tumor tissues (200× magnification). b. Positive immunohistochemistry in tumor tissues (200× magnification). c. Phosphate buffer saline (PBS) instead of primary antibody incubation was selected as negative control (200× magnification). d. Phosphate buffer saline (PBS) instead of primary antibody incubation was selected as negative control (200× magnification). D. Correlation between SPHK2 expression and overall survival in patients with HSCC. The red line represent the survival rate of patients in the positive expression group, the blue line represents the survival rate of patients in the negative expression group. Abbreviations: N, normal tissues; NL, tumor tissue without LN metastasis; L, tumor tissue with LN metastasis.

patients with LNM, compared to patients without LNM ($P < 0.05$) (**Figure 1A**, **1B**). To determine the localization of the SPHK2 protein, we conducted IHC analysis. As shown in **Figure 1C**, positive SPHK2 expression was characterized by a tan- or yellowish-stained cytoplasm whereas negative SPHK2 expression was seen as light blue-stained cytoplasm. Approximately 61.54% (24/39) of patients with LNM showed positive SPHK2 staining while only 46.67% of patients without LNM showed positive SPHK2 staining. These results indicate significantly increased SPHK2 levels in patients with LNM compared with those without LNM (**Table 2**, $P < 0.05$). The association between SPHK2 levels and the clinicopathological profiles of 57 HSCC

patients was then determined. As depicted in **Table 3**, the SPHK2 content was only associated with the LNM stage ($P < 0.001$), and not with sex, age, tumor stage, or degree of tumor differentiation. We also employed the Kaplan-Meier log-rank test to evaluate the survival curves related to the SPHK2 levels. Our findings revealed that HSCC patients with significantly elevated SPHK2 levels experienced worse survival (HR=3.597; 95% CI, 1.410-9.176, $P < 0.05$) (**Figure 1D**). Together, these findings indicated that SPHK2 contributed significantly to LNM and HSCC patient prognosis and that it was an independent risk factor for LNM and staging in HSCC patients.

Table 2. Immunohistochemical measurement of SPHK2 expression in HSCC tissue

Tissue	Number of patients	Expression of SPHK2		P Value
		Positive	Negative	
Lymphatic metastasis	39	24	15	P < 0.001***
Non-lymphatic metastasis	15	7	8	

Note: ***P values are from χ^2 test or Fisher's exact test and were statistically significant when < 0.001.

Table 3. Relationship between SPHK2 expression and clinicopathological features of HSCC

Clinicopathologic Factors	Number of patients	Expression of SPHK2		P Value
		Positive	Negative	
Gender				
Male	56	31	25	0.554
Female	1	0	1	
Age				
≤ 60	26	14	12	0.942
> 60	31	17	14	
Differentiation				
Poor	13	7	6	0.984
Moderate	28	16	12	
Good	13	7	6	
T stage				
I+II	12	6	6	0.328
III+IV	45	30	15	
N stage				
0+1	23	4	19	P < 0.001***
2+3	31	26	5	

Note: ***P values are from χ^2 test or Fisher's exact test and were statistically significant when < 0.001. Abbreviations: T stage, tumor stage; N stage, lymph node stage.

Influence of SPHK2 overexpression and knockdown on FaDu cell proliferation, migration, and invasion

To elucidate the role of SPHK2 in HSCC, we overexpressed and silenced SPHK2 expression in an HSCC cell line (FaDu) using lentiviral transduction, and analyzed its effect on cell physiology. The SPHK2 mRNA and protein levels were measured after transduction with different plasmids. Both SPHK2 mRNA and protein levels were markedly increased in FaDu cells transduced with lv-SPHK2, relative to the lv-NC and blank controls (P < 0.001, **Figure 2A**). In contrast, the SPHK2 mRNA and protein levels were significantly reduced in FaDu cells with sh-SPHK2, relative to sh-NC and blank controls (P < 0.001, **Figure 2B**). These results indicate the successful induction of SPHK2 overexpression and silencing in FaDu cells using lentiviral transduction.

We next examined the SPHK2-mediated regulation of FaDu cell proliferation, invasion, and migration using CCK-8, colony formation, and Transwell assays. As illustrated in **Figure 2C-G**, lv-NC, and sh-NC did not affect FaDu cell proliferation, invasion, or migration. In contrast, SPHK2 overexpression strongly enhanced FaDu cell proliferation, invasion, and migration relative to the lv-NC-transfected cells. Silencing of SPHK2, however, significantly reduced FaDu cell proliferation, invasion, and migration relative to the sh-NC-transfected cells. These findings indicated that SPHK2 overexpression enhanced HSCC proliferation and invasion whereas SPHK2 deficiency produced the opposite effect.

SPHK2 knockdown inhibits murine tumor development and LNM

To further verify the role of SPHK2 in mediating tumor malignancy, we conducted *in vivo* experi-
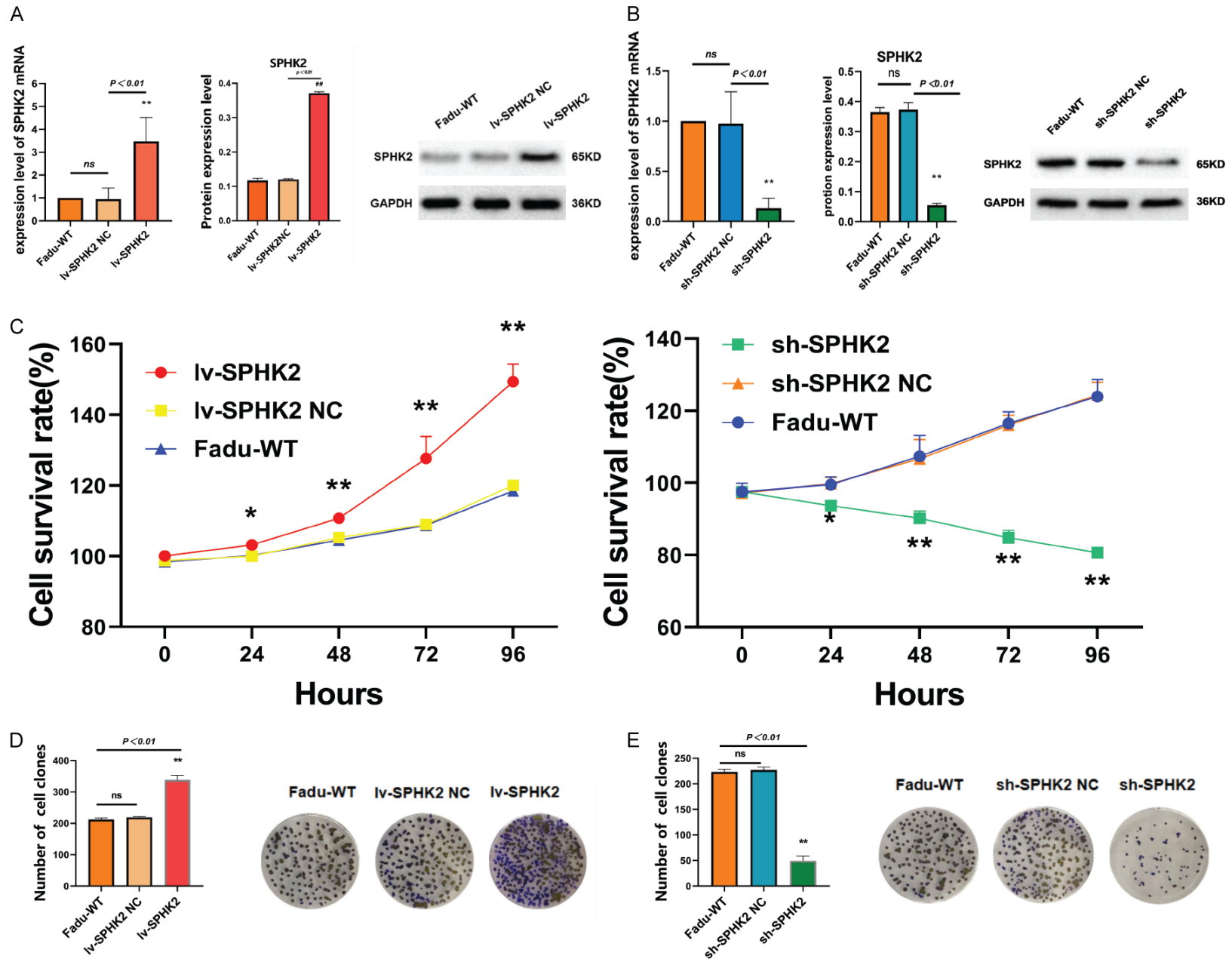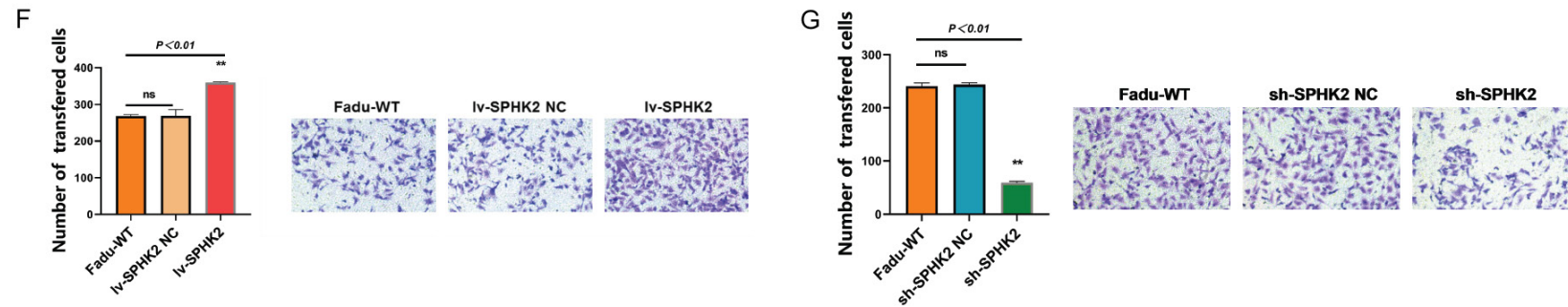
Figure 2. Changes in FaDu cell function after SPHK2 over-expression and silencing. A. SPHK2 mRNA and protein levels in SPHK2-over-expression FaDu cells; B. SPHK2 mRNA and protein levels in SPHK2-silenced FaDu cells; C. The CCK8 staining assay was used to measure the cell viability of FaDu cells at 24 h, 48 h, 72 h and 96 h, after transfection, respectively; D, E. The proliferation of FaDu cells was determined by colony formation assay; F, G. Transwell assay was used to determine the migration and invasion abilities of FaDu cells (200× magnification after 24 h). Abbreviations: Notes: ns P > 0.05, P < 0.05, *P < 0.001. Abbreviations: Fadu-WT, Wild-type Fadu cell lines; lv-SPHK2 NC, Overexpression of negative control lentiviral plasmids; lv-SPHK2, Overexpression of SPHK2 cell line transfected with lentivirus; sh-SPHK2 NC, silencing of negative control lentiviral plasmids; sh-SPHK2, silencing of SPHK2 cell line transfected with lentivirus.
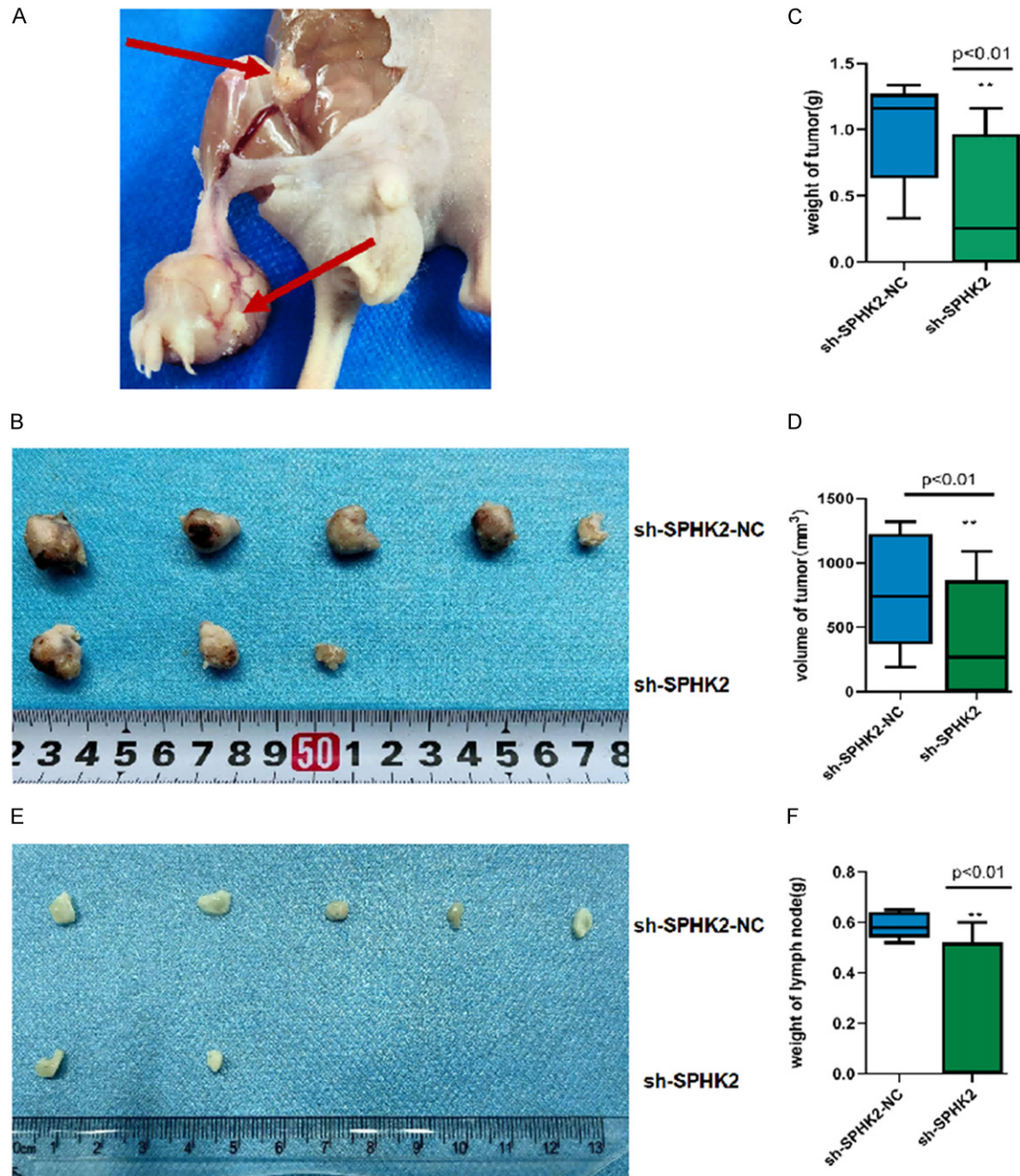
Figure 3. The tumor model of foot pad was established in nude mice. A. The tumor model of foot pad was established in nude mice, using a Fadu cell line stably transfected with sh-sphk2-NC and sh-sphk2, grossly after 35 days; B. Naked eye view of isolated tumour; C. Naked eye view of isolated metastatic inguinal lymph nodes; D. The weight of tumer; E. The volume of tumor; F. The weight of lymph node.

ments. Thirty-five days after tumor cell administration, the mice were euthanized and the tumor growth was assessed. This showed that the tumor growth in the primary foci of the foot pads of control mice was more rapid than that in the SPHK2-deficient mice (**Figure 3A**, **3B**). The tumor weights and volumes were then measured (**Figure 3C**). Tumor growth was observed to be greater in the control mice, seen in increased tumor weights and volumes, relative to the SPHK2-knockdown mice (P < 0.01, **Figure 3D**). We next examined the LNM in the popliteal fossa (**Figure 3E**), observing an LNM rate of 100% (4/4) in control mice and

50% (2/4) in the SPHK2-silenced mice (P < 0.001). Moreover, the lymph node weights in the control mice were significantly greater compared to those of the SPHK2-silenced mice (P < 0.01, **Figure 3F**). These findings confirmed that SPHK2 knockdown inhibited tumor development and LNM.

Expression of PI3K/AKT pathway

To identify the mechanism underlying the SPHK2-mediated regulation of LNM in HSCC, we performed bioinformatics analysis using the TCGA database. In all, 522 HSCC samples were divided into high- and low-expression cohorts, using the median SPHK2 level as the threshold. GO enrichment of the identified DEGs between the two cohorts was then performed. This showed that biological functions were enriched in the B cell receptor network (**Figure 4A**). It is well established that the B cell receptor network is an upstream mediator of the PI3K/AKT axis. To further verify its role in HSCC, we examined the expression of components of the PI3K/AKT axis using WB. This showed that the PI3K p110α, p-AKT 308, and p-AKT 473 protein levels were markedly enhanced in the lv-SPHK2-transfected cells versus the controls (**Figure 4B**). In contrast, the expression of PI3K and AKT was significantly reduced in the sh-SPHK2-transfected versus the control cells (**Figure 4C**). In addition, we examined the expression of each target protein in the tumor specimens obtained from animal experiments using WB. We verified the target proteins of the pathway and observed that the protein expression of PI3K110α, p-AKT308, and p-AKT473 was reduced in the sh-SPHK2 group compared to the blank plasmid control group (**Figure 4D**). These findings indicated that SPHK2 overexpression stimulated the PI3K/AKT axis whereas SPHK2 knockdown suppressed it. Moreover, the malignant behavior of SPHK2 in tumors was potentially associated with the PI3K/AKT axis.

The miR-19a-3p-mediated regulation of SPHK2 and its effect on SPHK2 function

We next assessed the role of miRNAs in the signaling network. Three databases, namely, miRTarBase, TarBase, and TargetScan, were searched to identify SPHK2-interacting miRNAs. This showed that miR-19a-3p and miR-19b-3p were common to all search results and were likely to be significant SPHK2-interacting

miRNAs (**Figure 5A**). Subsequent analysis showed that both miR-19a-3p and SPHK2 had complementary binding sites (**Figure 5B**) while miR-19B-3p did not. Immunofluorescence showed that miR-19a-3p abrogated SPHK2 activity in the wild-type but not mutant SPHK2 (**Figure 5C**). We next conducted q-PCR to assess miR-19a-3p levels in HSCC versus normal tissues finding that miR-19a-3p levels were substantially reduced in HSCC tissues relative to normal tissues. Moreover, the levels were also reduced in HSCC tissues with LNM, as opposed to HSCC tissues without LNM metastases (**Figure 5D**). Combined with our prior results (**Figure 1A**, **1B**), we hypothesized that miR-19a-3p may negatively regulate SPHK2 expression in HSCC. Hence, we next verified the association between miR-19a-3p and SPHK2 by successfully knocking down miR-19a-3p in FaDu cells, finding that miR-19a mRNA expression was markedly reduced, as expected, resulting in a marked increase in the SPHK2 protein content in sh-miR-19a cells, relative to the controls (sh-miR-19a NC) (**Figure 5E**). The levels of components of the PI3K/AKT axis were then assessed by WB. This showed that the sh-miR-19a-transfected cells exhibited relatively enhanced SPHK2 protein levels, as well as increased expression of PI3K110α, p-AKT308, and p-AKT473 relative to the controls (sh-miR-19-NC) (**Figure 5F**). The physiological activities in the transfected cells were then evaluated. As shown in **Figure 5G**, **5H**, the sh-miR-19-NC-transfected cells showed no change in FaDu cell proliferation, invasion, and migration. In contrast, the miR-19a-3p-deficient FaDu cells exhibited markedly enhanced proliferation, invasion, and migration, relative to controls. Taken together, these results confirmed that miR-19a-3p was negatively associated with SPHK2 protein to reduce its function. Furthermore, miR-19a-3p knockdown enhanced SPHK2 expression, activated the PI3K/AKT axis, and accelerated tumor proliferation, invasion, and migration.

SPHK2 knockdown and PI3K/AKT inhibitor counteract the effects of miR-19a knockdown

Given that miR-19a negatively modulates SPHK2 action, we further confirmed its effect by knocking down SPHK2 expression in miR-19a-deficient FaDu cells. To do this, we generated the following FaDu cell lines using lentiviral transduction: cells transfected with (1) the blank miR-19a plasmid (NC-sh-miR), (2) the miR-19a knockdown plasmid (sh-miR-19a), (3)
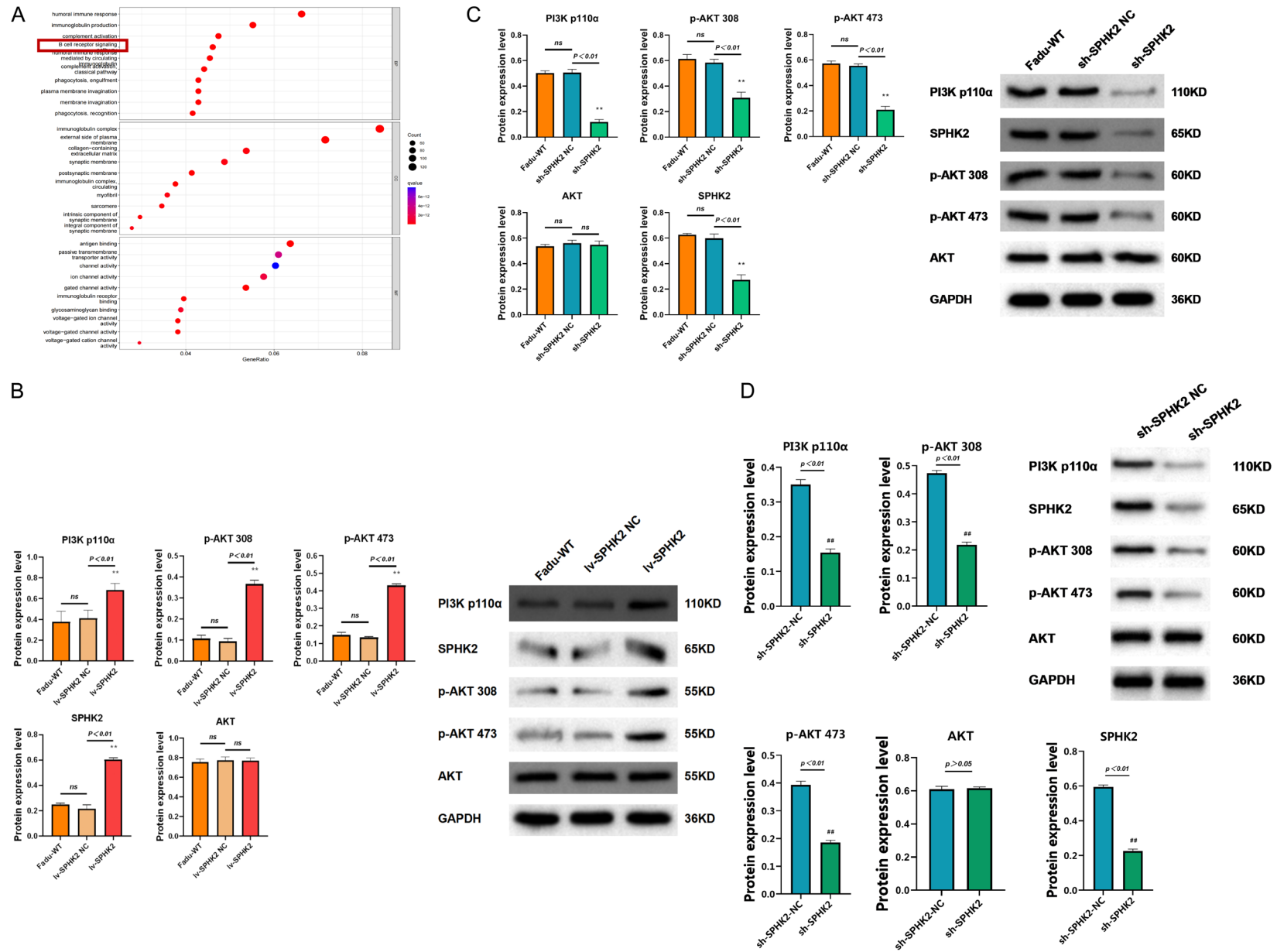
Figure 4. In vivo and vitro experiments to validate the effect of SPHK2 on the PI3K/AKT pathway. A. KEGG pathway enrichment analysis; B, C. Expression of each target protein of PI3K/AKT pathway in different cell lines; D. PI3k/akt pathway was investigated in animal experimental tumors.
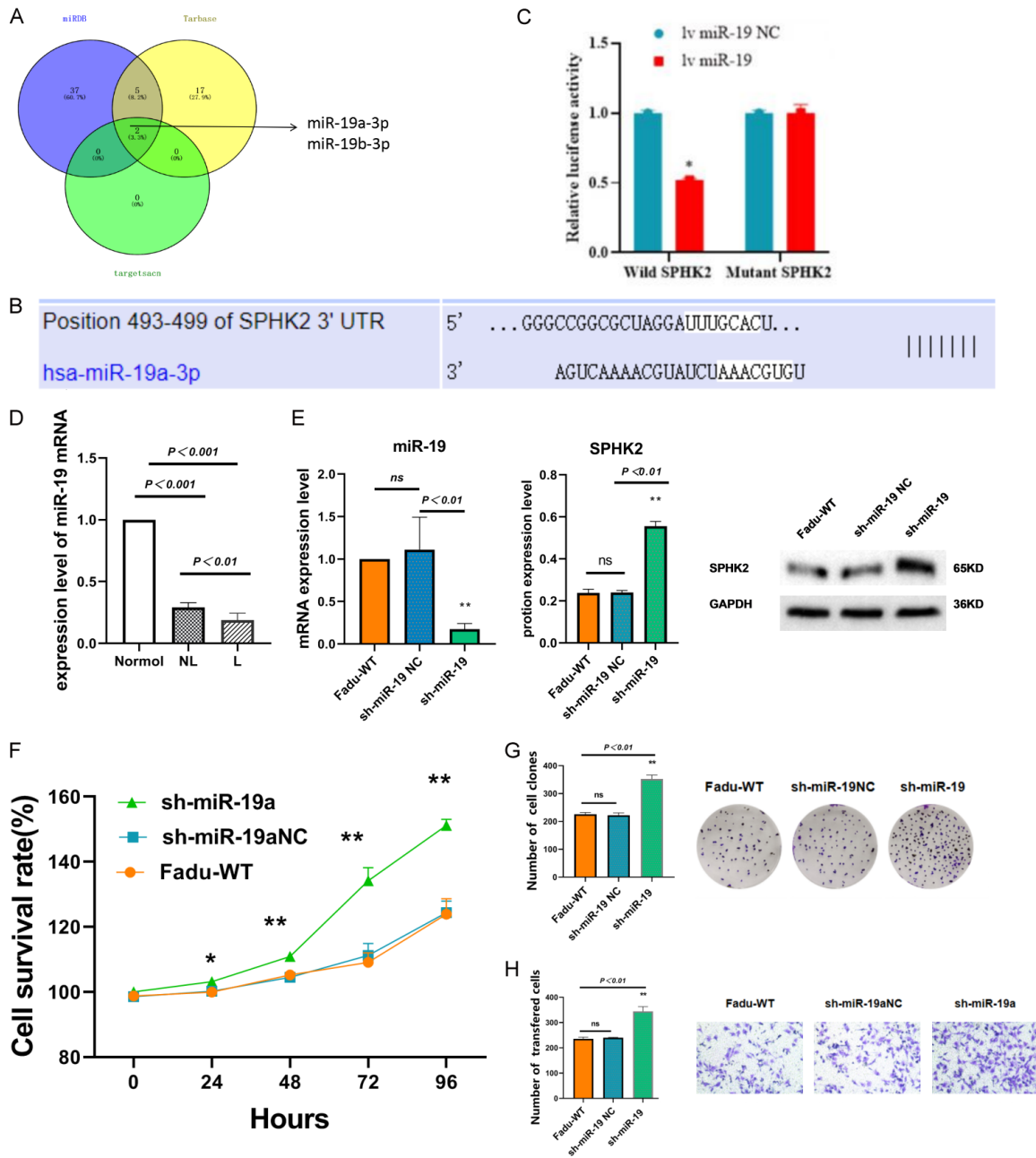
Figure 5. Changes in FaDu cell function after miR-19a silencing. A. Venn diagram of SPHK2 targeting miRNAs based on 3 databases: miRTarBase, TarBase and targetsacn; B. Binding site between miR-19a-3p and SPHK2; C. Immu-nofluorescence test results; D. mRNA expression levels of miR-19a were detected by qRT-PCR in HSCC tissues (10 samples from HSCC patients with LN metastasis patients and another 10 from patients without LN metastasis) and 10 corresponding adjacent normal tissues; E. miR-19a mRNA and SPK2 protein levels in mrR-19a-silenced FaDu cells; F. The CCK8 staining assay was used to measure the cell viability of FaDu cells at 24 h, 48 h, 72 h and 96 h, after transfection, respectively; G. The proliferation of FaDu cells was determined by colony formation assay; H. Transwell assay was used to determine the migration and invasion abilities of FaDu cells (200× maanification after 24 h).

miR-19a knockdown + SPHK2 blank plasmids (sh-miR-19a + NC-sh-SPHK2), and (4) miR-19a + SPHK2 knockdown (sh-miR-19a + sh-SPHK2). Subsequently, we repeated the physiological and PI3K/AKT axis-related protein assessments.
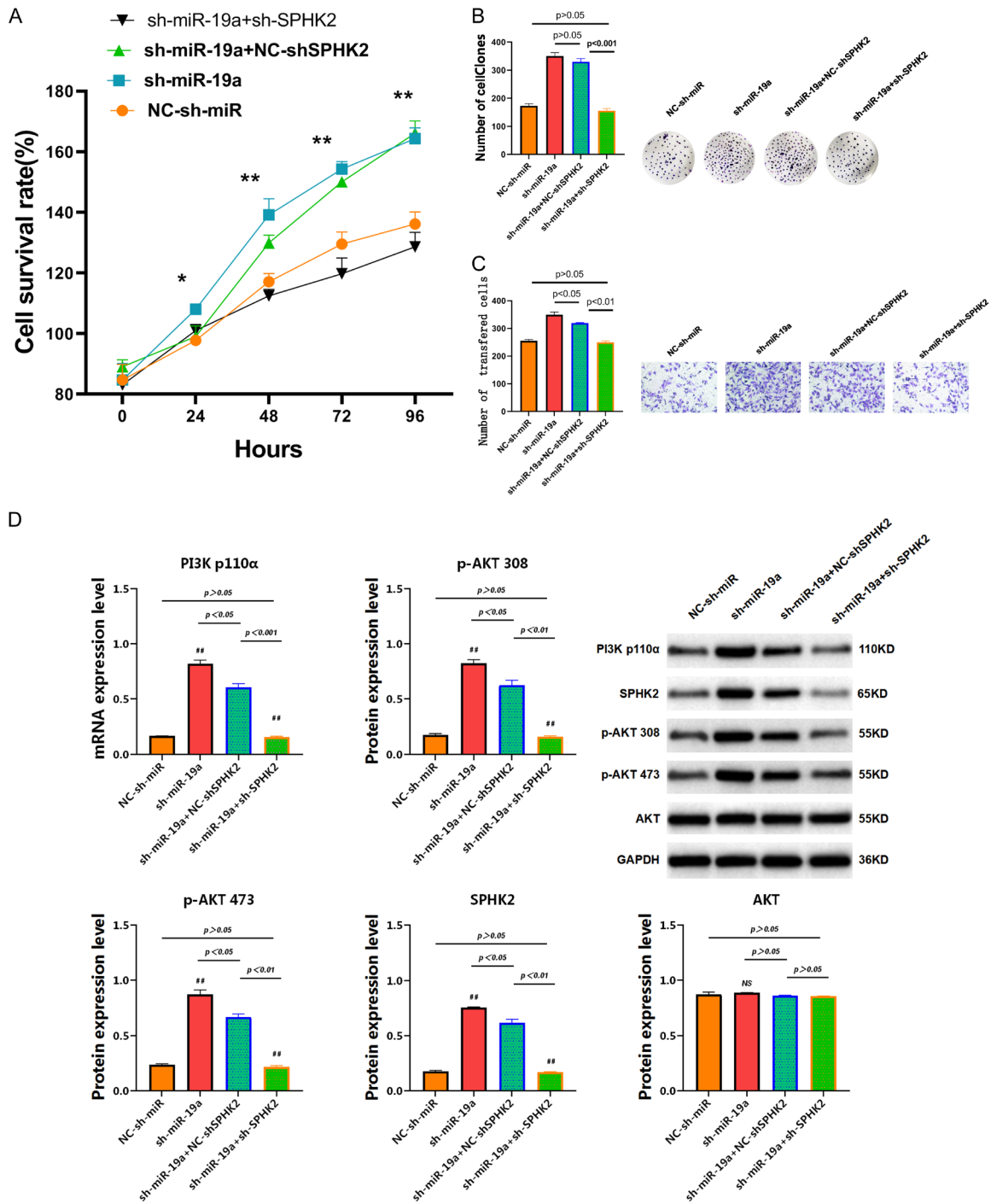
Figure 6. The silent SPHK2 rescued to changes in cell function induced by silencing mir-19a. A. The CCk8 staining assay was used to measure the cell viability of FaDu cells at 24 h, 48 h, 72 h and 96 h, after transfection, respectively; B. The proliferation of FaDu cells was determined by colony formation assay; C. Transwell assay was used to determine the migration and invasion abilities of FaDu cells (200× magnification after 24 h); D. Expression of each target protein of PI3K/AKT pathway in different cell lines.

As shown in **Figure 6**, sh-miR-19a- and sh-miR-19a + NC-sh-SPHK2-transfected FaDu cells showed increased proliferation, invasion, and migration, as well as enhanced PI3K110α, p-AKT308, and p-AKT473 protein expression, relative to the NC-sh-miR-transfected cells.
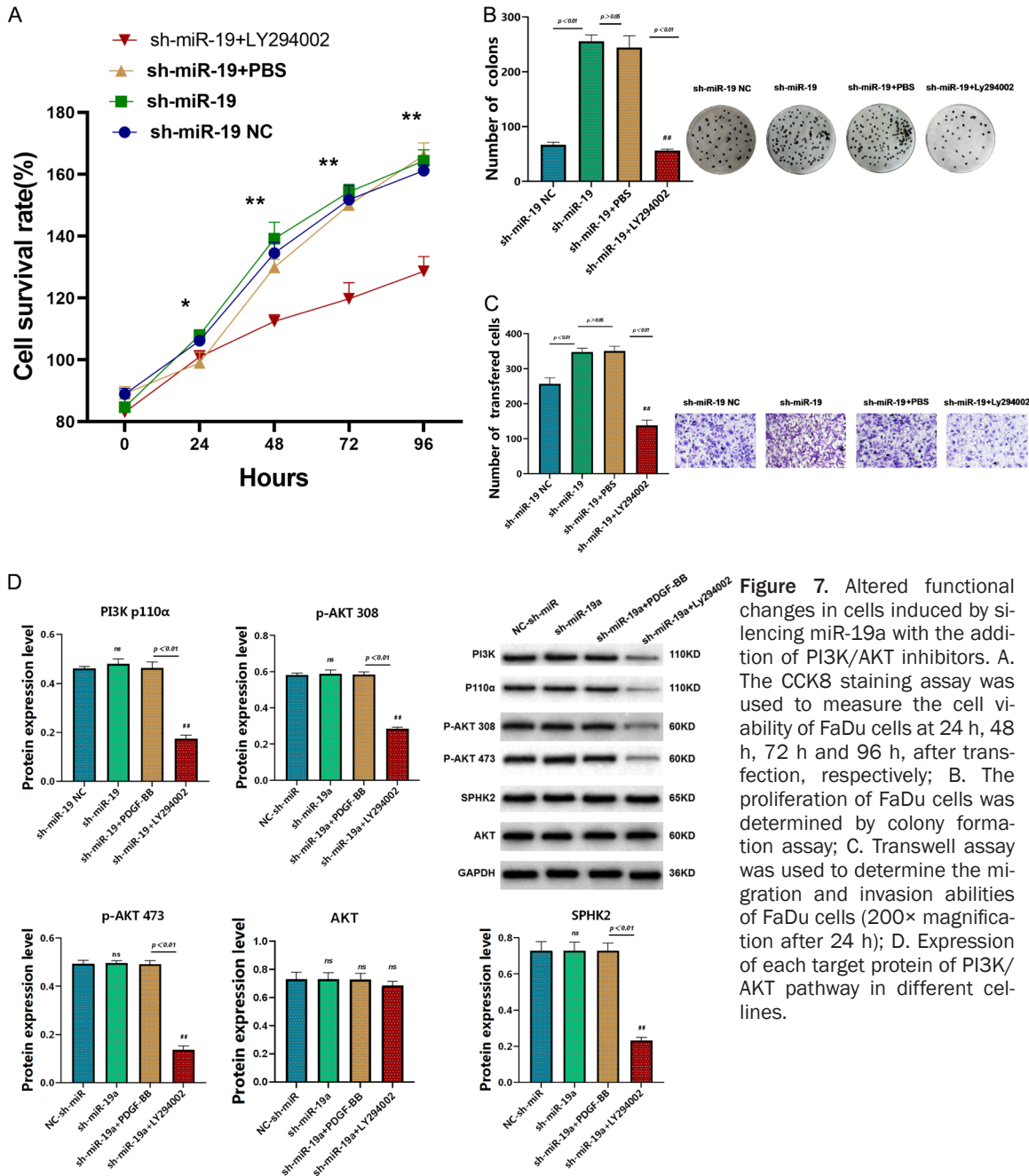
Figure 7. Altered functional changes in cells induced by silencing miR-19a with the addition of PI3K/AKT inhibitors. A. The CCK8 staining assay was used to measure the cell viability of FaDu cells at 24 h, 48 h, 72 h and 96 h, after transfection, respectively; B. The proliferation of FaDu cells was determined by colony formation assay; C. Transwell assay was used to determine the migration and invasion abilities of FaDu cells (200× magnification after 24 h); D. Expression of each target protein of PI3K/AKT pathway in different cell-lines.

However, after simultaneous knockdown of SPHK2 and miR-19a (sh-miR-19a + sh-SPHK2), there was no significant difference from the wild-type.

Furthermore, to support the conclusion that SPHK2 was regulated by miR-19a-3p to modulate tumor proliferation and invasion via the PI3K/AKT axis, we examined the proliferation and invasion ability of sh-miR-19a-3p-HSCC cells treated with a PI3K/AKT inhibitor. We us-

ed a PI3K/AKT inhibitor to construct four cell lines: FaDu cells + silent miR-19a blank plasmid transfection group (sh-miR-19 NC), silent miR-19a group (sh-miR-19), silent miR-19a group + PBS (sh-miR-19 + PBS), and the silenced miR-19a group + PI3K inhibitor (sh-miR-19 + LY294002) for cloning, proliferation, invasion, and cell survival experiments.

As shown in **Figure 7A-C**, compared with the blank plasmid transfection group (sh-miR-19

NC), the silent miR-19a group (sh-miR-19a) showed increased colony formation, proliferation, invasion, and cell survival, and could activate the PI3K/AKT pathway (**Figure 7D**). After addition of the PI3K inhibitor, it was seen that the silent miR-19a group + PI3K inhibitor (sh-miR-19 + LY294002) showed significantly reduced colony formation, proliferation, and viability. Regarding the expression of the pathway target proteins, the addition of PI3K/AKT inhibitor was seen to significantly inhibit PI3K p110α, pAKT307, and pAKT308 ($P < 0.01$), while no significant effect was seen on the expression of SPHK2 ($P > 0.05$). This experiment indicates that the addition of PIK3K/AKT inhibitor successfully inhibited the expression of the downstream PI3K p110α, pAKT307, and pAKT308, while having little effect on the expression of SPHK2. Cell function experiments showed that the inhibition of PI3K/AKT reversed the silencing of miR-19a-3p in cell survival, proliferation, and migration. This assay further established that miR-19a-3p can affect cell survival, proliferation, and invasive migration functions via the PI3K/AKT axis in the FaDu cell line.

Discussion

HSCC is a highly malignant tumor and thus represents a serious threat to human life and health [1]. The current form of HSCC management is surgery. However, the 5-year OS rate has not seen much improvement in the past decade. Several investigations have shown that the incidence of LNM in HSCC patients is approximately 60-80%, and the 5-year OS rate in HSCC patients with LNM is 40% lower, compared to patients without LNM [5, 6]. This suggests that LNM may be the main contributor to treatment failure in HSCC patients. Here, we explored the factors affecting LNM in HSCC patients to pave way for the development of appropriate screening indicators and treatment strategies for HSCC with LNM.

In a prior investigation, we used whole-transcriptome sequencing to identify DEGs between HSCC patients with or without LNM. These DEGs included ANXA6, TBC1D14, IGF2BP2, and Raf-1 [25, 35-38], and SPHK2 was selected as a strongly upregulated DEG. Recent studies have reported that the SPHK2-mediated regulation of cell apoptosis depends primarily on its intracellular localization. When expressed in the cytoplasm, SPHK2 inhibits apoptosis and promotes cell proliferation [39]. On translocation to the nucleus, SPHK2 enhances apoptosis and suppresses cell proliferation [40, 41]. These experiments confirmed that SPHK2 is highly expressed in HSCC patients, acting as a pro-oncogene, and is mainly expressed in the tumor cell cytoplasm. Moreover, HSCC patients with LNM exhibited higher levels of SPHK2 than HSCC patients without LNM. It was also found that elevated SPHK2 expression was an independent risk factor for HSCC patient prognosis, and was closely associated with the LNM stage. This is the first time that the relationship between SPHK2 and HSCC has been described. It was found that SPHK2 was differentially expressed in HSCC and that SPHK2 expression correlated with patient survival, indicating the value of SPHK2 as a prognostic indicator. We further confirmed in both in vitro and in vivo experiments that inhibition of SPHK2 expression effectively reduced the development of primary tumor foci and lymphatic metastasis. These results are consistent with the previous trends observed in the patient samples. Collectively, these results suggested that SPHK2 can serve as an essential bioindicator of LNM diagnosis and HSCC patient prognosis.

Finally, we explored the mechanisms whereby SPHK2 affects HSCC. The PI3K/AKT axis is a classical signaling pathway that is critical for tumor pathology, and it is overactivated in a variety of tumor cells. Several studies have reported a strong association between the PI3K axis and processes affecting tumor outcome, namely, angiogenesis, autophagy, apoptosis, and the EMT [42, 43]. The bioinformatics analysis showed, for the first time, that SPHK2 can regulate PI3K/AKT pathway while experimental verification confirmed that SPHK2 can activate the PI3K/AKT pathway, that knockdown of SPHK2 can inhibit the PI3K/AKT pathway, and thus that the oncogenic behavior of SPHK2 in tumors may be related to the PI3K/AKT pathway. Specifically, we investigated upstream microRNAs (miRNAs). Recent investigations revealed marked disturbances in miR-19a-3p expression in cancer tissues, as well as in other diseases or pathological states. Aberrant miR-19a-3p expression was found to be a potential risk factor for worse patient outcome in multiple human malignancies. Additionally, abnormal miR-19a-3p levels are

correlated with the incidence of LNM [44]. Currently, there is no shortage of evidence involving the association between miR-19a-3p-mediated tumor regression and the AKT axis. The PI3K/AKT axis is a classical signaling pathway that is critical for tumor pathology, and it is overexpressed in a variety of tumor cells. We confirmed reduced expression of miR-19a-3p in patients with HSCC. Furthermore, we showed that miR-19a-3p was differentially expressed in HSCC patients with and without LNM and that miR-19a-3p was able to bind to SPHK2 and thus negatively regulate SPHK2 expression by inhibiting its translation. Cellular experiments, moreover, confirmed that silencing miR-19a-3p promoted SPHK2 expression, activated the PI3K/AKT pathway, and promoted tumor survival, proliferation, and invasive migration.

Due to time issues, we were unable to validate SPHK2 prospectively as a predictor of prognosis in HSCC patients. Nevertheless, we have clearly demonstrated that SPHK2 functions as an oncogene in HSCC and its expression is closely related to patient survival and the presence or absence of LNM, exhibiting biological properties through the activation of the PI3K/AKT axis. On the other hand, miR-19a-3p, as an upstream target of SPHK2, was also found to correlate with the presence or absence of LNM in HSCC patients and showed oncogenic properties in HSCC by suppressing SPHK2 expression and thus the PI3K/AKT axis. In future investigations, we plan to explore inhibitors of SPHK2 and miR-19a-3p for the suppression of tumor development and LNM in mouse models of HSCC to provide a theoretical basis for the development of targeted tumor therapy.

Acknowledgements

Disclosure of conflict of interest

None.

Address correspondence to: Dr. Guohua Hu, Department of Otorhinolaryngology, The First Affiliated Hospital of Chongqing Medical University, No. 1 Youyi Road, Yuzhong District, Chongqing 400016, China. E-mail: hghcq@sina.com

References

[1] Ahn D, Kim JH, Sohn JH, Sin CM and Lee JE. Laryngeal preservation in stage III/IV resectable laryngo-hypopharyngeal squamous cell carcinoma following concurrent chemoradiotherapy with capecitabine/cisplatin. Mol Clin Oncol 2013; 1: 685-691.

[2] Li M, Lorenz RR, Khan MJ, Burkey BB, Adelstein DJ, Greskovich JF Jr, Koyfman SA and Scharpf J. Salvage laryngectomy in patients with recurrent laryngeal cancer in the setting of nonoperative treatment failure. Otolaryngol Head Neck Surg 2013; 149: 245-251.

[3] Buckley JG and MacLennan K. Cervical node metastases in laryngeal and hypopharyngeal cancer: a prospective analysis of prevalence and distribution. Head Neck 2000; 22: 380-385.

[4] Cooper JS, Porter K, Mallin K, Hoffman HT, Weber RS, Ang KK, Gay EG and Langer CJ. National cancer database report on cancer of the head and neck: 10-year update. Head Neck 2009; 31: 748-758.

[5] Roberts TJ, Colevas AD, Hara W, Holsinger FC, Oakley-Girvan I and Divi V. Number of positive nodes is superior to the lymph node ratio and American Joint Committee on Cancer N staging for the prognosis of surgically treated head and neck squamous cell carcinomas. Cancer 2016; 122: 1388-1397.

[6] Gobbetti T and Cooray SN. Annexin A1 and resolution of inflammation: tissue repairing properties and signalling signature. Biol Chem 2016; 397: 981-993.

[7] Szklarczyk D, Morris JH, Cook H, Kuhn M, Wyder S, Simonovic M, Santos A, Doncheva NT, Roth A, Bork P, Jensen LJ and von Mering C. The STRING database in 2017: quality-controlled protein-protein association networks, made broadly accessible. Nucleic Acids Res 2017; 45: D362-D368.

[8] Sanchez-Vega F, Mina M, Armenia J, Chatila WK, Luna A, La KC, Dimitriadoy S, Liu DL, Kantheti HS, Saghafinia S, Chakravarty D, Daian F, Gao Q, Bailey MH, Liang WW, Foltz SM, Shmulevich I, Ding L, Heins Z, Ochoa A, Gross B, Gao J, Zhang H, Kundra R, Kandoth C, Bahceci I, Dervishi L, Dogrusoz U, Zhou W, Shen H, Laird PW, Way GP, Greene CS, Liang H, Xiao Y, Wang C, Iavarone A, Berger AH, Bivona TG, Lazar AJ, Hammer GD, Giordano T, Kwong LN, McArthur G, Huang C, Tward AD, Frederick MJ, McCormick F, Meyerson M; Cancer Genome Atlas Research Network, Van Allen EM, Cherniack AD, Ciriello G, Sander C and Schultz N. Oncogenic signaling pathways in The Cancer Genome Atlas. Cell 2018; 173: 321-337, e10.

[9] Li Y, Lu T and Hu G. Gene sequencing and expression of Raf-1 in lymphatic metastasis of hypopharyngeal carcinoma. Cancer Biomark 2020; 28: 181-191.

[10] Schwalm S, Beyer S, Hafizi R, Trautmann S, Geisslinger G, Adams DR, Pyne S, Pyne N, Schaefer L, Huwiler A and Pfeilschifter J. Validation of highly selective sphingosine kinase 2 inhibitors SLM6031434 and HWG-35D as effective anti-fibrotic treatment options in a mouse model of tubulointerstitial fibrosis. Cell Signal 2021; 79: 109881.

[11] Couttas TA, Rustam YH, Song H, Qi Y, Teo JD, Chen J, Reid GE and Don AS. A novel function of sphingosine kinase 2 in the metabolism of sphinga-4, 14-diene lipids. Metabolites 2020; 10: 236.

[12] Liang J, Zhang X, He S, Miao Y, Wu N, Li J and Gan Y. Sphk2 RNAi nanoparticles suppress tumor growth via downregulating cancer cell derived exosomal microRNA. J Control Release 2018; 286: 348-357.

[13] Canlas J, Holt P, Carroll A, Rix S, Ryan P, Davies L, Matusica D, Pitson SM, Jessup CF, Gilbbins IL and Haberberger RV. Sphingosine kinase 2-deficiency mediated changes in spinal pain processing. Front Mol Neurosci 2015; 8: 29.

[14] Couttas TA, Kain N, Tran C, Chatterton Z, Kwok JB and Don AS. Age-dependent changes to sphingolipid balance in the human hippocampus are gender-specific and may sensitize to neurodegeneration. J Alzheimers Dis 2018; 63: 503-514.

[15] Shi W, Ma D, Cao Y, Hu L, Liu S, Yan D, Zhang S, Zhang G, Wang Z, Wu J and Jiang C. SphK2/S1P promotes metastasis of triple-negative breast cancer through the PAK1/LIMK1/cofilin1 signaling pathway. Front Mol Biosci 2021; 8: 598218.

[16] Pitman M, Oehler MK and Pitson SM. Sphingolipids as multifaceted mediators in ovarian cancer. Cell Signal 2021; 81: 109949.

[17] Huo FC, Zhu ZM, Zhu WT, Du QY, Liang J and Mou J. METTL3-mediated m6A methylation of SPHK2 promotes gastric cancer progression by targeting KLF2. Oncogene 2021; 40: 2968-2981.

[18] Zhang YH, Shi WN, Wu SH, Miao RR, Sun SY, Luo DD, Wan SB, Guo ZK, Wang WY, Yu XF, Cui SX and Qu XJ. SphK2 confers 5-fluorouracil resistance to colorectal cancer via upregulating H3K56ac-mediated DPD expression. Oncogene 2020; 39: 5214-5227.

[19] Xiao G, Wang Q, Li B, Wu X, Liao H, Ren Y and Ai N. MicroRNA-338-3p suppresses proliferation of human liver cancer cells by targeting SphK2. Oncol Res 2018; 26: 1183-1189.

[20] Wang H, Zhao B, Bian E, Zong G, He J, Wang J, Ma C and Wan J. Ubiquitination destabilizes protein sphingosine kinase 2 to regulate glioma malignancy. Front Cell Neurosci 2021; 15: 660354.

[21] Xue Y, Jiang K, Ou L, Shen M, Yang Y, Lu J and Xu W. Targeting sphingosine kinase 1/2 by a novel dual inhibitor SKI-349 suppresses non-small cell lung cancer cell growth. Cell Death Dis 2022; 13: 602.

[22] Aoki M and Fujishita T. Oncogenic roles of the PI3K/AKT/mTOR axis. Curr Top Microbiol Immunol 2017; 407: 153-189.

[23] Lien EC, Dibble CC and Toker A. PI3K signaling in cancer: beyond AKT. Curr Opin Cell Biol 2017; 45: 62-71.

[24] Ediriweera MK, Tennekoon KH and Samarakoon SR. Role of the PI3K/AKT/mTOR signaling pathway in ovarian cancer: Biological and therapeutic significance. Semin Cancer Biol 2019; 59: 147-160.

[25] Shorning BY, Dass MS, Smalley MJ and Pearson HB. The PI3K-AKT-mTOR pathway and prostate cancer: at the crossroads of AR, MAPK, and WNT signaling. Int J Mol Sci 2020; 21: 4507.

[26] Ni QF, Zhang Y, Yu JW, Hua RH, Wang QH and Zhu JW. miR-92b promotes gastric cancer growth by activating the DAB2IP-mediated PI3K/AKT signalling pathway. Cell Prolif 2020; 53: e12630.

[27] Zhang F, Li K, Pan M, Li W, Wu J, Li M, Zhao L and Wang H. miR-589 promotes gastric cancer aggressiveness by a LIFR-PI3K/AKT-c-Jun regulatory feedback loop. J Exp Clin Cancer Res 2018; 37: 152.

[28] Kolenda T, Guglas K, Kopczyńska M, Sobocinska J, Teresiak A, Blizniak R and Lamperska K. Good or not good: role of miR-19a in cancer biology. Rep Pract Oncol Radiother 2020; 25: 808-819.

[29] Ardizzone A, Calabrese G, Campolo M, Filippone A, Giuffrida D, Esposito F, Colarossi C, Cuzzocrea S, Esposito E and Paterniti I. Role of

miRNA-19a in cancer diagnosis and poor prognosis. Int J Mol Sci 2021; 22: 4697.

[30] Zhao Y and Li A. miR-19b-3p relieves intervertebral disc degeneration through modulating PTEN/PI3K/Akt/mTOR signaling pathway. Aging (Albany NY) 2021; 13: 22459-22473.

[31] Liu Y, Liu R, Yang F, Cheng R, Chen X, Cui S, Gu Y, Sun W, You C, Liu Z, Sun F, Wang Y, Fu Z, Ye C, Zhang C, Li J and Chen X. miR-19a promotes colorectal cancer proliferation and migration by targeting TIA1. Mol Cancer 2017; 16: 53.

[32] Wu K, Feng J, Lyu F, Xing F, Sharma S, Liu Y, Wu SY, Zhao D, Tyagi A, Deshpande RP, Pei X, Ruiz MG, Takahashi H, Tsuzuki S, Kimura T, Mo YY, Shiozawa Y, Singh R and Watabe K. Exosomal miR-19a and IBSP cooperate to induce osteolytic bone metastasis of estrogen receptor-positive breast cancer. Nat Commun 2021; 12: 5196.

[33] Paiva MM, Kimura ET and Coltri PP. miR18a and miR19a recruit specific proteins for splicing in thyroid cancer cells. Cancer Genomics Proteomics 2017; 14: 373-381.

[34] Feng Y, Liu J, Kang Y, He Y, Liang B, Yang P and Yu Z. miR-19a acts as an oncogenic microRNA and is up-regulated in bladder cancer. J Exp Clin Cancer Res 2014; 33: 67.

[35] Yu D, Pan M, Li Y, Lu T, Wang Z, Liu C and Hu G. RNA N6-methyladenosine reader IGF2BP2 promotes lymphatic metastasis and epithelial-mesenchymal transition of head and neck squamous carcinoma cells via stabilizing slug mRNA in an m6A-dependent manner. J Exp Clin Cancer Res 2022; 41: 6.

[36] Lu T, Li Y, Pan M, Yu D, Wang Z, Liu C and Hu G. TBC1D14 inhibits autophagy to suppress lymph node metastasis in head and neck squamous cell carcinoma by downregulating macrophage erythroblast attacher. Int J Biol Sci 2022; 18: 1795-1812.

[37] Li Y, Lu T and Hu G. Gene sequencing and expression of Raf-1 in lymphatic metastasis of hypopharyngeal carcinoma. Cancer Biomark 2020; 28: 181-191.

[38] Li L, Wang Z, Lu T, Li Y, Pan M, Yu D and Hu G. Expression and functional relevance of ANXA1 in hypopharyngeal carcinoma with lymph node metastasis. Onco Targets Ther 2021; 14: 1387-1399.

[39] Zi D, Zhou ZW, Yang YJ, Huang L, Zhou ZL, He SM, He ZX and Zhou SF. Danusertib induces apoptosis, cell cycle arrest, and autophagy but inhibits epithelial to mesenchymal transition involving PI3K/Akt/mTOR signaling pathway in human ovarian cancer cells. Int J Mol Sci 2015; 16: 27228-27251.

[40] Kma L and Baruah TJ. The interplay of ROS and the PI3K/Akt pathway in autophagy regulation. Biotechnol Appl Biochem 2022; 69: 248-264.

[41] Yu FB, Sheng J, Yu JM, Liu JH, Qin XX and Mou B. MiR-19a-3p regulates the Forkhead box F2-mediated Wnt/β-catenin signaling pathway and affects the biological functions of colorectal cancer cells. World J Gastroenterol 2020; 26: 627-244.

[42] Peng Y, Huang D, Ma K, Deng X and Shao Z. MiR-19a as a prognostic indicator for cancer patients: a meta-analysis. Biosci Rep 2019; 39: BSR20182370.

[43] Wang W, Hao Y, Zhang A, Yang W, Wei W, Wang G and Jia Z. miR-19a/b promote EMT and proliferation in glioma cells via SEPT7-AKT-NF-κB pathway. Mol Ther Oncolytics 2021; 20: 290-305.

[44] Liu R, Shen L, Qu N, Zhao X, Wang J and Geng J. MiR-19a promotes migration and invasion by targeting RHOB in osteosarcoma. Onco Targets Ther 2019; 12: 7801-7808.